SYNTHETIC BIOLOGY

Integrated translation and metabolism in a partially self-synthesizing biochemical network

Simone Giaveri[1]*†, Nitin Bohra[1,2]†, Christoph Diehl[1], Hao Yuan Yang[1,2], Martine Ballinger[1], Nicole Paczia[3], Timo Glatter[4], Tobias J. Erb[1,5]*

One of the hallmarks of living organisms is their capacity for self-organization and regeneration, which requires a tight integration of metabolic and genetic networks. We sought to construct a linked metabolic and genetic network in vitro that shows such lifelike behavior outside of a cellular context and generates its own building blocks from nonliving matter. We integrated the metabolism of the crotonyl-CoA/ethyl-malonyl-CoA/hydroxybutyryl-CoA cycle with cell-free protein synthesis using recombinant elements. Our network produces the amino acid glycine from CO_2 and incorporates it into target proteins following DNA-encoded instructions. By orchestrating ~50 enzymes we established a basic cell-free operating system in which genetically encoded inputs into a metabolic network are programmed to activate feedback loops allowing for self-integration and (partial) self-regeneration of the complete system.

Self-organization, regeneration, and repair are key properties of all living systems. Cells solve this challenge through a tight integration of metabolic and genetic networks (*1*, *2*). Genetic networks encode the components of metabolic networks which in turn provide the energy and building blocks to execute the genetic programs for self-regulation and self-regeneration (*3*). Construction of systems showing similar functionalities is one of the milestones on the way to construction of synthetic cells and is also key to development of biotechnological systems that are capable of decision-making, self-optimization, and Darwinian evolution (*4*).

Recent efforts in synthetic biology have pioneered cell-free transcription-translation (TX-TL) systems that are able to process genetic programs (*5*, *6*), respond to organic input molecules (*7*), and (partially) self-regenerate when supplemented with instructions, energy, and building blocks (*8*, *9*). At the same time, several complex metabolic networks have been successfully reconstructed outside of a cellular context (*10*–*18*). These in vitro networks were combined with energy modules (*19*, *20*) to produce different metabolites, including organic acids and more complex molecules from simple precursors such as glucose or CO_2 (*21*).

However, so far such genetic and metabolic in vitro systems have not been integrated with each other to achieve higher-order functionality. We aimed to develop a metabolic and genetic linked network in which both layers recursively communicate with one another. This link is achieved through an essential amino acid (glycine), which is autonomously synthesized from inorganic carbon (CO_2) through the metabolic network and controls the output of the genetic network, which itself feeds back to the metabolic layer through DNA-encoded instructions.

To realize such a system, we sought to combine a 16-enzyme in vitro CO_2-fixation system, the crotonyl-CoA/ethyl-malonyl-CoA/hydroxybutyryl-CoA (CETCH) cycle (*10*), with a cell-free TX-TL system (PURE) for protein production (*22*). The CETCH cycle converts CO_2 into glyoxylate by transforming the C3 metabolite propionyl-CoA through incorporation of two CO_2 molecules into the C5 intermediate methylmalyl-CoA, which is recycled back into propionyl-CoA and the C2 output glyoxylate. We sought to convert glyoxlyate further into glycine and incorporate it into target proteins through the TX-TL machinery of the PURE system. With these proteins, we envisioned establishment of recursive feed-forward loops to the metabolic network, which would allow the production of key enzymes of the CETCH cycle (Fig. 1A).

Realizing a genetic network that is controlled by in vitro production of glycine

To construct our interlinked network, we first established a PURE TX-TL mix lacking glycine (Δgly-PURE TX-TL) in which externally added glycine is required for protein production. We provided this Δgly-PURE TX-TL system with a DNA template encoding for the green fluorescent protein EGFP (*23*) and supplemented it with increasing concentrations of glycine (Fig. 1B). Fluorescence read-out showed a linear dependency between 10 μM and 150 μM glycine, confirming that the concentration of glycine directly controls EGFP production in the Δgly-PURE system. At concentrati beyond 150 μM glycine (e.g., 300 μM), output signal was saturated.

Next, we tested whether glycine could be produced in situ in the Δgly-PURE system from externally added glyoxylate (the product of the CETCH cycle). We sought to employ a transamination of glyoxylate by accessing the large pool of potassium glutamate (100 mM) of the PURE system and using glutamate-glyoxylate aminotransferase (GGT1) from *Arabidopsis thaliana* (*24*) or the promiscuous aspartate-glyoxylate aminotransferase (BhcA) from *Paracoccus denitrificans* (*25*) as a transaminating enzyme (Fig. 1C).

We tested either aminotransferase in a reaction mixture with 100 μM pyridoxal phosphate (PLP), 300 μM glyoxylate, 100 mM potassium ^{15}N-glutamate, and all 19 proteinogenic amino acids (at 300 μM each) and followed the formation of ^{15}N-labeled and unlabeled glycine with high-performance liquid chromatography-mass spectrometry (HPLC-MS/MS). GGT1 produced 217 ± 15 μM ^{15}N-glycine after 15 min and only minor amounts of unlabeled glycine (Fig. 1D), demonstrating that glutamate served as the exclusive amino donor for GGT1. By contrast, BhcA produced 201 ± 6 μM ^{15}N-glycine and 40 ± 3 μM unlabeled glycine (fig. S3), indicating that other amino acids (i.e., aspartic acid, see fig. S3) were used by BhcA. We chose to continue with GGT1 and integrated the transaminase into a Δgly-PURE TX-TL system with EGFP as a fluorescent readout, adding different concentrations of glyoxylate. Similar to the experiments with externally added glycine, we observed a linear dependence of EGFP production from glyoxylate in the range of 10 to 150 μM glyoxylate (Fig. 1E). These results confirmed that glyoxylate could indeed serve as a link between the CETCH cycle and Δgly-PURE TX-TL system.

In the following, we tested the effect of coenzymes, cofactors, salts, and buffers of the CETCH cycle onto the productivity of the Δgly-PURE TX-TL system. We decided for a version of the CETCH cycle (CETCH vA7) that was recently optimized by active learning (*26*) and investigated the effect of different concentrations of the individual CETCH cycle components onto cell-free TX-TL. This identified $MgCl_2$ and ATP as the most critical compounds that influenced the final yield and kinetics of EGFP production, respectively (fig. S11). We then added all CETCH components—except for the starting substrate propionyl-CoA—to a Δgly-PURE TX-TL system with 300 μM glycine and EGFP as readout. When testing different ratios of the CETCH cycle and Δgly-PURE TX-TL, 25 μl of PURE reaction mixture containing 5 μl of CETCH worked best (Fig. 1F), demonstrating that the Δgly-PURE system can in principle be coupled with a 1:4 v/v diluted CETCH cycle.

[1]Department of Biochemistry and Synthetic Metabolism, Max Planck Institute for Terrestrial Microbiology, Marburg, Germany. [2]Max Planck School Matter to Life, Heidelberg, Germany. [3]Core Facility for Metabolomics and Small Molecule Mass Spectrometry, Max Planck Institute for Terrestrial Microbiology, Marburg, Germany. [4]Facility for Mass Spectrometry and Proteomics, Max Planck Institute for Terrestrial Microbiology, Marburg, Germany. [5]SYNMIKRO Center for Synthetic Microbiology, Marburg, Germany.
*Corresponding author. Email: toerb@mpi-marburg.mpg.de (T.J.E); simone.giaveri@mpi-marburg.mpg.de (S.G.)
†These authors contributed equally to this work.

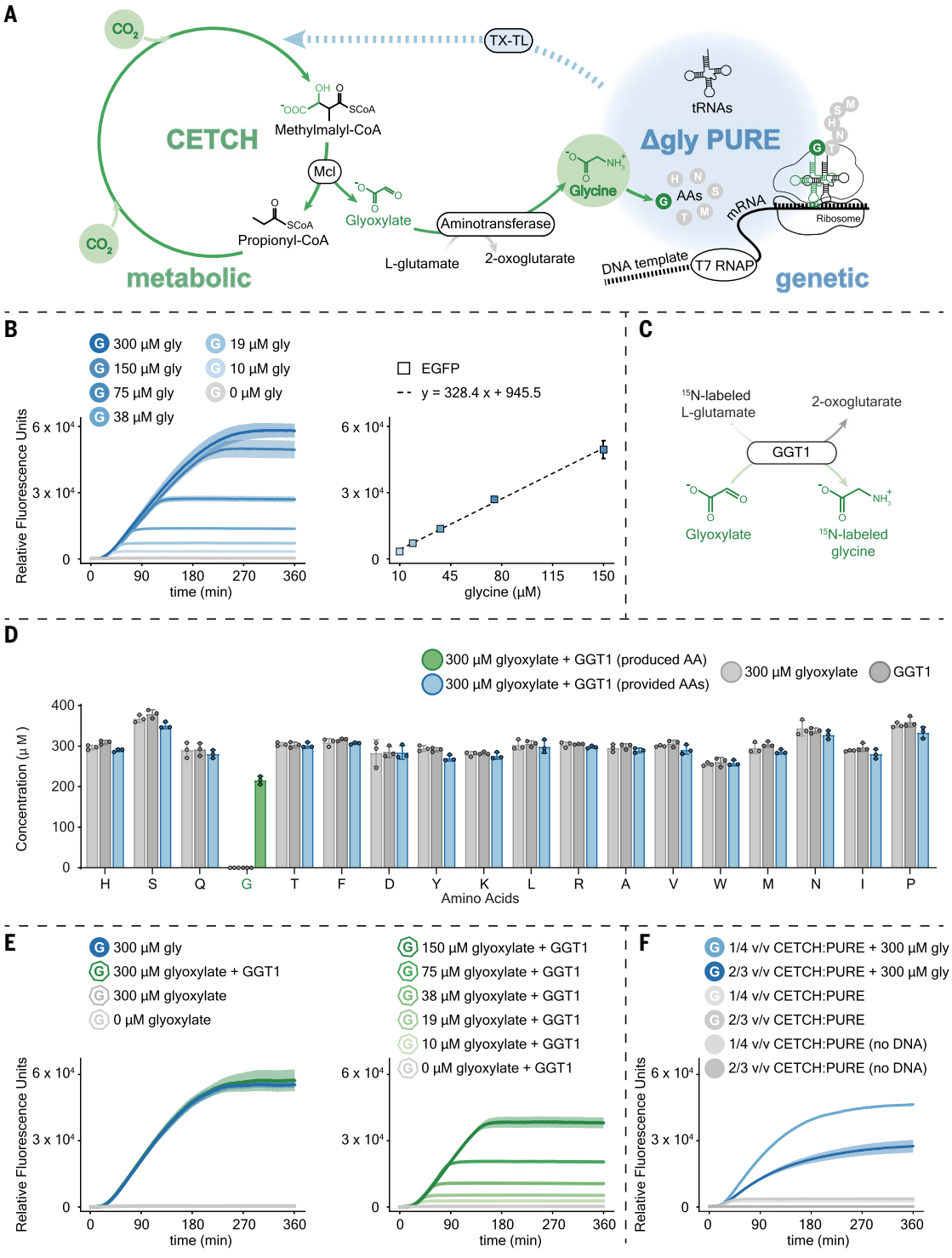

Fig. 1. Realization of an in vitro genetic network that depends on in vitro metabolism. (**A**) Schematic of the topology of the metabolic and genetic linked network described in this study, where the metabolic layer of the CETCH cycle (green) is integrated with the genetic layer of the PURE system (blue) by the transamination of the product of CO_2 fixation (glyoxylate) into an amino acid (glycine); glycine is used in turn by TX-TL to produce key enzymes for CO_2 fixation. See fig. S1 and table S1 for a comprehensive representation of the system and for enzyme abbreviations, respectively. (**B**) (Left) Fluorescent signal resulting from the cell-free expression of the *EGFP* template in Δgly-PURE TX-TL system with different concentrations of externally added glycine (blue curves). Negative controls without glycine were included (gray curves). (Right) Plot of the linear dependence between glycine concentration and fluorescence read-out. (**C**) Scheme of the transamination reaction of glyoxylate into ^{15}N-glycine by ^{15}N-glutamate and GGT1 aminotransferase from *A. thaliana*. (**D**) Bar graph representing the amino acid analysis by HPLC-MS/MS of the result of the transamination reaction sketched in (C), performed in presence of GGT1, glyoxylate, ^{15}N-glutamate, and 19 proteinogenic amino acids (glycine omitted), for 15 min (produced ^{15}N-glycine is indicated by the green bar and provided AAs are indicated by the blue bars) at 30°C. Negative control assays without GGT1 (light gray bars), or glyoxylate (dark gray bars) were included. Comprehensive data of the amino acid analysis are reported in figs. S3, S4, S5, S6, and S7. (**E**) Fluorescent signal resulting from the cell-free expression of *EGFP* template in Δgly-PURE TX-TL system with GGT1 and different concentrations of externally added glyoxylate (green curves). Negative controls without glyoxylate or without GGT1 were performed (gray curves). A reference control with glycine (blue curve) was included. (**F**) Fluorescent signal resulting from the cell-free expression of *EGFP* template in a Δgly-PURE TX-TL system supplemented with glycine in the presence of different concentrations of CETCH components without propionyl-CoA (blue curves). Negative controls without propionyl-CoA and glycine or without propionyl-CoA and DNA templates (gray curves) were performed. All TX–TL reactions were incubated at 37°C into the microplate reader with gain as 100. TX–TL reactions were run in triplicate; expression curves represent the statistical mean of the results at any acquisition time; shading represent the standard deviation of the same data. Bar plots of the statistical mean of the results (triplicates) are shown; error bars represent the standard deviation of the same data.

Optimizing the metabolic network that produces glycine from CO_2

We next tested whether a 1:4 v/v diluted CETCH cycle could produce sufficient glycine in the presence of 100 mM potassium glutamate and GGT1. HPLC-MS/MS analysis showed that a diluted CETCH that started with 200 μM propionyl-CoA produced 552 ± 27 μM glycine at 30°C within 4 hours (Fig. 2A). This activity corresponded to a CO_2-fixation efficiency η_{CO2} of 5.5 ± 0.3 (η_{CO2} is defined as CO_2 equivalents fixed per acceptor molecule), which is comparable to earlier published versions of the CETCH cycle (e.g., CETCH v5.4) (*10*).

We continued by stepwise supplementation of the 1:4 v/v diluted CETCH cycle with additional components of the Δgly-PURE TX-TL system, to identify any factors that would affect η_{CO2} (Fig. 2A). Upon addition of the reducing agents dithiothreitol (DTT), or Tris(2-carboxyethyl)phosphine (TCEP), η_{CO2} decreased slightly to moderately (5.1 ± 0.3 for DTT; 3.6 ± 0.2 for TCEP). By contrast, supplementation with magnesium acetate (11.8 mM) severely decreased η_{CO2} to 0.8 ± 0.02, indicating a strong negative interaction between system components. We hypothesized that acetate could serve as an alternative substrate for 4-hydroxybutyryl-CoA synthetase, thus reducing flux through the CETCH cycle (*27*). To overcome this limitation we replaced magnesium acetate with hemi-magnesium glutamate (*28*) and also removed any residual acetate in the ribosome and TX-TL enzyme fractions of the Δgly-PURE system through buffer exchange, which increased η_{CO2} significantly to 2.8 ± 0.04, corresponding to the production of 275 ± 4 μM glycine within 4 hours (Fig. 2A).

Finally, we investigated how varying concentrations of the starting substrate propionyl-CoA would affect η_{CO2} of the 1:4 v/v diluted CETCH cycle. Decreasing propionyl-CoA concentrations from 200 to 50 μM decreased total glycine production from 275 ± 4 μM to 183 ± 7 μM but more than doubled the η_{CO2} from 2.8 ± 0.04 to 7.3 ± 0.3 (Fig. 2B). This data indicated that the 1:4 v/v diluted CETCH cycle turned more efficiently at lower propionyl-CoA concentrations, which is in line with recent findings (*18*).

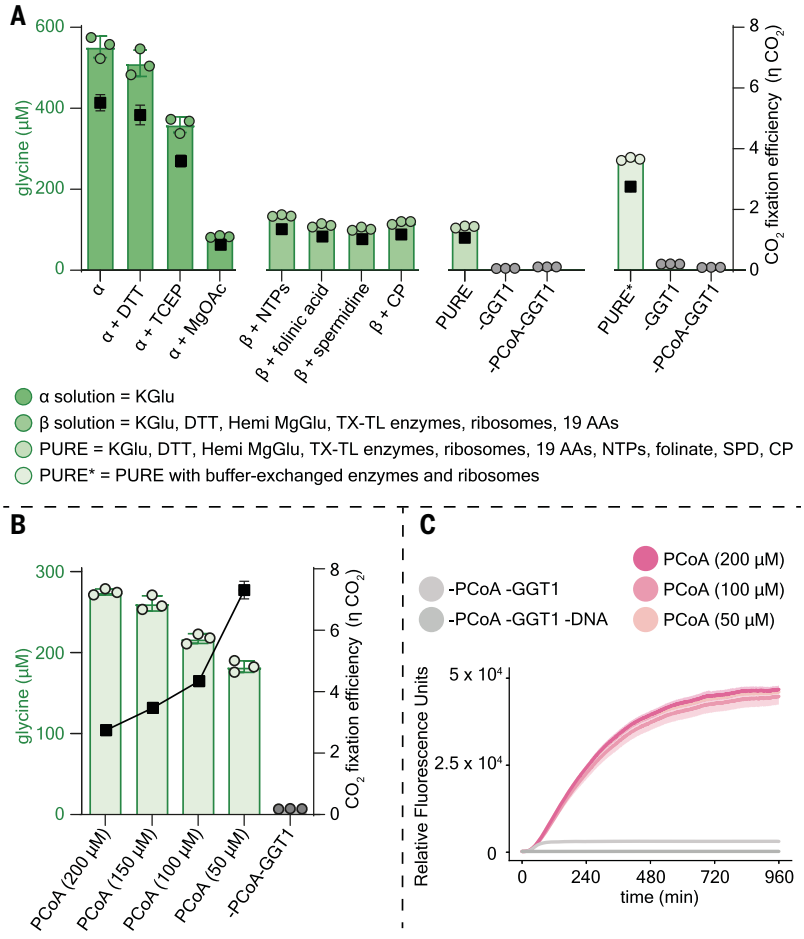

Fig. 2. CO_2 fixation into glycine by the CETCH cycle supplemented with Δgly-PURE TX-TL system. (**A**) Left *y*-axis: bar graph representing the absolute concentration of glycine, measured by HPLC-MS/MS produced over the course of 4 hours at 30°C by the CETCH cycle started with 200 μM propionyl-CoA and stepwise-supplemented with the components of the Δgly-PURE TX-TL system (green bars). Negative controls without GGT1 or without propionyl-CoA and GGT1 were included (gray bars). Right *y*-axis: CO_2-fixation efficiency η_{CO2} of the CETCH cycle (black squares). A detailed description of the reaction assembly is reported in table S5. (**B**) Left *y*-axis: bar graph representing the absolute concentration of glycine, measured by HPLC-MS/MS, produced over the course of 4 hours at 30°C by the CETCH cycle in the presence of the Δgly-PURE TX-TL system and started with different concentrations of propionyl-CoA (green bars). Right *y*-axis: CO_2-fixation efficiency η_{CO2} of the CETCH cycle (black squares). (**C**) Fluorescent signal resulting from the cell-free expression of *EGFP* template in Δgly-PURE TX-TL system added with the CETCH cycle and different concentrations of propionyl-CoA (pink curves). Negative controls without propionyl-CoA and GGT1 (light gray curve) or without DNA templates (dark gray curve) were performed. TX–TL reactions were incubated at 30°C into the microplate reader with gain as 100. TX–TL reactions were run in triplicate; expression curves represent the statistical mean of the results at any acquisition time; shading represents the standard deviation of the same data. Bar plots of the statistical mean of the results (triplicates) are shown; error bars represent the standard deviation of the same data.

Interlinking the metabolic and genetic networks for (self-)integration and regeneration

Having optimized the working conditions of the metabolic (CETCH cycle) and genetic (Δgly-PURE TX-TL) layers independently and reciprocally, we aimed at operating both systems together at 30°C, i.e., the optimized temperature for the CETCH cycle (fig. S10). We combined the 16 enzymes of the CETCH cycle with the 36 enzymes of the Δgly-PURE TX-TL system, added GGT1, and supplemented the reaction mix with ribosomes, as well as all other coenzymes, cofactors, and salts required. We activated the metabolic layer with different concentrations of propionyl-CoA (50, 100, and 200 μM, respectively) and the genetic layer with a DNA template encoding for EGFP. Under these conditions EGFP production above background was only observed when GGT1 was present (converting glyoxylate produced by the CETCH cycle into glycine used by Δgly-PURE TX-TL). Moreover, these results confirmed that 50 μM propionyl-CoA was sufficient and optimal for EGFP production (Fig. 2C). Higher concentrations of the starting substrate did not further improve the EGFP signal, which is in line with earlier experiments that showed EGFP signal saturation above 150 μM glycine (Fig. 1, B and E). Altogether, these experiments showed the successful integration of the metabolic and genetic networks into one in vitro system.

We next envisioned a "self-integrating" network in which the metabolic and genetic layers are linked through a feed-forward loop. We assembled a ΔGGT1 network (i.e., a system missing the enzyme GGT1, which links both

layers) and designed a feed-forward loop based on GGT1, which we provided as DNA-based template to a PURE TX-TL system together with an EGFP readout (Fig. 3A). In the presence of 10 μM glycine, EGFP was produced at relevant concentrations, only when the CETCH cycle was started with propionyl-CoA (Fig. 3B), or when external glyoxylate (300 μM) was provided (fig. S12). These data confirmed that the metabolic and genetic layers of the ΔGGT1 network were successfully linked in an autocatalytic fashion, which made the system independent from the initial glycine input (fig. S19).

Inspired by the ability of living cells to self-construct and self-maintain, we sought to further integrate our metabolic and genetic networks to achieve "self-regeneration" in vitro. To this end, we selected the CETCH cycle enzyme ethylmalonyl-CoA mutase (Ecm) that converts ethylmalonyl-CoA into methylsuccinyl-CoA (fig. S1). We produced Ecm by TX-TL in the PURE system (fig. S9) and verified enzyme activity by coexpressing *Ecm* and *EGFP* templates in a Δgly-PURE TX-TL system supplemented with 100 μM ethylmalonyl-CoA, CETCH components (see Methods), and 10 μM glycine (fig. S13). Next, we assembled a ΔEcm network, a system that is missing Ecm and is dependent on (partial) self-regeneration of Ecm to become metabolically active and autonomously

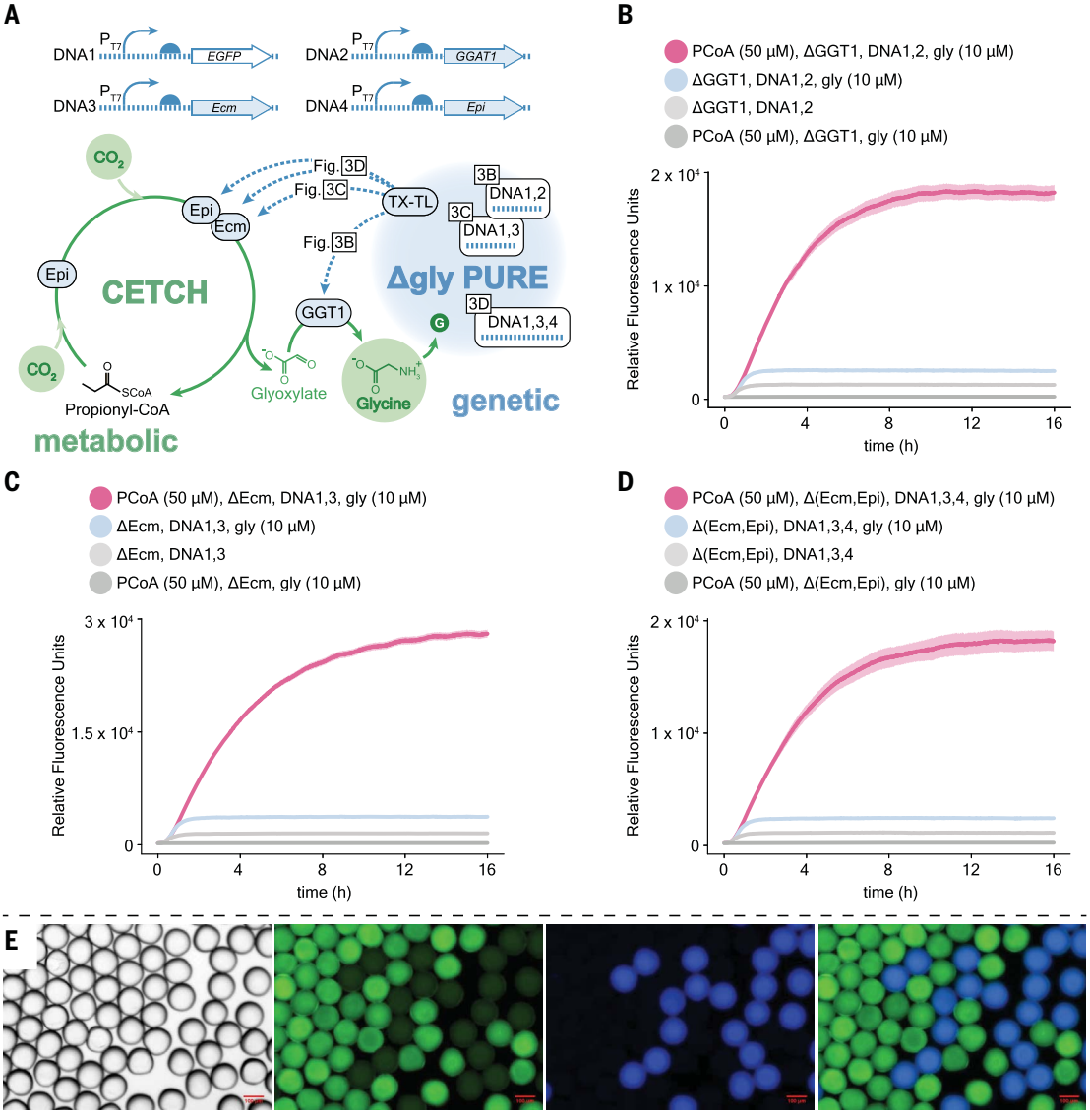

Fig. 3. Interdependent metabolic and genetic networks. (**A**) Schematic summarizing the topology of the "self-integrating" (**B**) and "self-regenerating" (**C** and **D**) networks. (B to D) Plots of the fluorescence signal resulting from the expression of *EGFP* template in a microplate reader. The pink curves are obtained by supplementing (B) the ΔGGT1 network with *GGAT1* and *EGFP* templates, (C) the ΔEcm network with *Ecm* and *EGFP* templates, (D) the in Δ(Ecm,Epi) network with *Ecm*, *Epi* and *EGFP* templates, and with 50 μM propionyl-CoA and 10 μM glycine. Negative controls without propionyl-CoA (blue curves) or without propionyl-CoA and glycine (light gray curves) or without DNA templates (dark gray curves) were included. TX–TL reactions were incubated at 30°C into the microplate reader, with gain as 100. TX–TL reactions were run in triplicate; expression curves represent the statistical mean of the results at any acquisition time; shading represents the standard deviation of the same data. (**E**) Micrographs of a synthetic organelle mimic able to increase its CO_2 fixation autonomously in micrometer-size droplets through bottom-up assembling a self-regenerating ΔEcm network. Droplets with *Ecm* and *EGFP* DNA templates or without DNA (negative control) were incubated at 30°C and imaged after 6 hours. The negative control droplets population was barcoded with Cascade Blue™ hydrazide trilithium salt dye. From left to right: brightfield image of the micrometer-size droplets, sample droplet population (GFP channel), negative control droplet population (DAPI channel), overlay of the images acquired in GFP and DAPI channels. Scale bars are 100 μm.

synthesize glycine from CO_2. Upon feeding the ΔEcm network with the DNA sequences encoding for Ecm (and EGFP), 50 μM propionyl CoA, and minimal glycine concentrations (10 μM), the network became functional and remained active for ~12 hours (compared to the control, which showed only ~1 hour of activity), continuously converting CO_2 into glycine which in turn enabled continuous production of Ecm (Fig. 3, A and C, and fig. S15). Proteomic analysis using $NaH^{13}CO_3$ indeed verified that most of the glycine residues in Ecm (and EGFP) were synthesized from CO_2 (fig. S16).

We ultimately aimed to assemble a metabolic and genetic linked network able to regenerate multiple enzymes of the metabolic layer. To this end, we selected methylmalonyl-/ethylmalonyl-CoA epimerase (Epi) that catalyzes the racemization of methylsuccinyl-CoA following the Ecm reaction in the CETCH cycle (fig. S1). We produced Epi by cell-free TX-TL (fig. S9) and verified enzyme activity as described above (see Methods and fig. S14). Next, we assembled a Δ(Ecm,Epi) network (i.e., a network that lacks two subsequent steps of the metabolic layer). Only upon providing the system with DNA sequences, propionyl CoA, and minimal concentrations of glycine did the system become and remain able to (partially) self-regenerate and produce the enzymes for a key step of the CETCH cycle from CO_2 (Fig. 3, A and D).

Finally, to test whether in vitro self-regeneration can also be performed in cell-sized compartments, we attempted to miniaturize and spatially confine these interactions in microfluidic-generated water-in-oil droplets (Fig. 3E). To this end, we produced a binary emulsion of the ΔEcm network and created two droplet populations with and without DNA. Only in presence of DNA were droplets able to perform CO_2 fixation by autonomously producing one of the key enzymes (Ecm) necessary for their own metabolism, demonstrating that the systems developed here were also functional on a cellular scale.

Conclusions

Overall, our efforts demonstrate how metabolism and gene expression can be integrated and simultaneously operated outside of their cellular context. Our system provides a step forward for the self-construction and self-maintenance of biological networks, hallmarks of living systems (*29*). Reconstructing such lifelike features in vitro provides the opportunity to construct "autonomous" cell-free systems in the future that can produce their own components autonomously when provided with energy and matter from the environment (*30*).

Although we successfully demonstrate the generation of one central building block (glycine) directly from inorganic carbon (CO_2) in this study, a number of challenges still remain when transitioning from such a "partial" self-regeneration toward a system that uses CO_2 as the sole carbon source for all organic molecules or when transitioning from regenerating a small number of enzymes to encode a complete metabolic network from DNA. Such efforts will likely profit from recent advancements and new concepts in cell-free biology, including the development of anaplerotic reaction sequences for replenishing metabolic intermediates (*11*), improving TX-TL synthesis rates, and genetic regulation (*8*, *31*).

One of the biggest challenges of operating complex in vitro systems is enzyme instability (*12*, *15*, *32*), as well as homeostatic maintenance against external perturbations. Our approach of coupling metabolic and genetic networks could extend the lifetime and robustness of such in vitro systems by programming "self-repair" and "dynamic adaptation" responses, which could be of use in biotechnology (e.g., maintenance of biocatalytic enzyme cascades) and disease control (e.g., production of bioactive molecules on-demand). Moreover, future efforts that integrate cell-free gene expression with multiple biosynthetic as well as catabolic modules could open new avenues for developing completely autonomous in vitro systems that are able to evolve (*30*).

REFERENCES AND NOTES

1. P. Schwille *et al.*, *Angew. Chem. Int. Ed.* **57**, 13382–13392 (2018).
2. S. Mann, *Angew. Chem. Int. Ed.* **52**, 155–162 (2013).
3. J. Zhu, C. B. Thompson, *Nat. Rev. Mol. Cell Biol.* **20**, 436–450 (2019).
4. S. Tror, S. Jeon, H. T. Nguyen, E. Huh, K. Shin, *Small Methods* **7**, e2300182 (2023).
5. N. Laohakunakorn *et al.*, *Front. Bioeng. Biotechnol.* **8**, 213 (2020).
6. D. Garenne *et al.*, *Nat. Rev. Methods Primers* **1**, 49 (2021).
7. A. Pandi *et al.*, *Nat. Commun.* **10**, 3880 (2019).
8. B. Lavickova, N. Laohakunakorn, S. J. Maerkl, *Nat. Commun.* **11**, 6340 (2020).
9. K. Hagino, N. Ichihashi, *ACS Synth. Biol.* **12**, 1252–1263 (2023).
10. T. Schwander, L. Schada von Borzyskowski, S. Burgener, N. S. Cortina, T. J. Erb, *Science* **354**, 900–904 (2016).
11. C. Diehl, P. D. Gerlinger, N. Paczia, T. J. Erb, *Nat. Chem. Biol.* **19**, 168–175 (2023).
12. S. Sundaram *et al.*, *Angew. Chem. Int. Ed.* **60**, 16420–16425 (2021).
13. D. L. Trudeau *et al.*, *Proc. Natl. Acad. Sci. U.S.A.* **115**, E11455–E11464 (2018).
14. M. Scheffen *et al.*, *Nat. Catal.* **4**, 105–115 (2021).
15. S. Luo *et al.*, *Nat. Catal.* **5**, 154–162 (2022).
16. R. McLean *et al.*, *Sci. Adv.* **9**, eadh4299 (2023).
17. T. Cai *et al.*, *Science* **373**, 1523–1527 (2021).
18. S. Luo *et al.*, *Nat. Catal.* **6**, 1228–1240 (2023).
19. T. E. Miller *et al.*, *Science* **368**, 649–654 (2020).
20. S. Luo *et al.*, *Joule* **7**, 1745–1758 (2023).
21. H. Taniguchi, K. Okano, K. Honda, *Synth. Syst. Biotechnol.* **2**, 65–74 (2017).
22. Y. Shimizu *et al.*, *Nat. Biotechnol.* **19**, 751–755 (2001).
23. S. Giaveri *et al.*, *Adv. Mater.* **33**, e2104581 (2021).
24. A. H. Liepman, L. J. Olsen, *Plant Physiol.* **131**, 215–227 (2003).
25. L. Schada von Borzyskowski *et al.*, *Nature* **575**, 500–504 (2019).
26. A. Pandi *et al.*, *Nat. Commun.* **13**, 3876 (2022).
27. M. Könneke *et al.*, *Proc. Natl. Acad. Sci. U.S.A.* **111**, 8239–8244 (2014).
28. K. Libicher, R. Hornberger, M. Heymann, H. Mutschler, *Nat. Commun.* **11**, 904 (2020).
29. K. P. Adamala *et al.*, *Nat. Rev. Mol. Cell Biol.* **25**, 162–167 (2024).
30. Z. Abil, C. Danelon, *Front. Bioeng. Biotechnol.* **8**, 927 (2020).
31. M. Levy, R. Falkovich, S. S. Daube, R. H. Bar-Ziv, *Sci. Adv.* **6**, eaaz6020 (2020).
32. N. Laohakunakorn, *Front. Bioeng. Biotechnol.* **8**, 788 (2020).

ACKNOWLEDGMENTS

We thank D.G. Marchal, P.D. Gerlinger, A. Sánchez-Pascuala, D. Schindler, and M. Tinzl for fruitful discussions. **Funding:** This work was supported by the Max Planck Society. S.G. is grateful to the European Molecular Biology Organization (EMBO) postdoctoral fellowship (ALTF 162-2022, to S.G.). N.B. and H.Y.Y. conducted their research within the Max Planck School Matter to Life supported by the German Federal Ministry of Education and Research (BMBF) in collaboration with the Max Planck Society. **Author contributions:** T.J.E. and S.G. conceived the work. S.G. designed the experiments; S.G., N.B., and T.J.E. discussed the results. S.G. and N.B. performed cloning, enzyme activity assays, cell-free TX-TL assays, CETCH assays, and metabolic and genetic assays; they also analyzed the data. C.D. and N.B. synthesized CoA-Thioesters. S.G., C.D., N.B., and H.Y.Y. performed protein production and purification. N.P. performed mass spectrometry for amino acid analysis; N.P., N.B., and S.G. analyzed the data. T.G. performed mass spectrometry for proteomics; T.G. and S.G. analyzed the data. M.B., N.B., and S.G. performed microfluidics experiments. T.J.E. supervised the work. S.G. and T.J.E. wrote the manuscript with contributions from all authors. **Competing interests:** The authors declare no competing interests. **Data and materials availability:** All data supporting the findings of this study are available within the article and the supplementary material.

SUPPLEMENTARY MATERIALS

science.org/doi/10.1126/science.adn3856
Materials and Methods
Figs. S1 to S19
Tables S1 to S7
MDAR Reproducibility Checklist
References (*33*–*35*)

Submitted 7 December 2023; accepted 3 June 2024
10.1126/science.adn3856